Acta Crystallographica Section F
Structural Biology and Crystallization Communications
ISSN 1744-3091

Structure of TTHA1623, a novel metallo-β-lactamase superfamily protein from *Thermus thermophilus* HB8

Akihiro Yamamura,[a] Akitoshi Okada,[a] Yasuhiro Kameda,[a] Jun Ohtsuka,[a] Noriko Nakagawa,[b,c] Akio Ebihara,[b] Koji Nagata[a,b] and Masaru Tanokura[a,b]*

[a]Department of Applied Biological Chemistry, Graduate School of Agricultural and Life Sciences, University of Tokyo, 1-1-1 Yayoi, Bunkyo-ku, Tokyo 113-8657, Japan, [b]RIKEN SPring-8 Center, Harima Institute, 1-1-1 Kouto, Sayo-cho, Sayo-gun, Hyogo 679-5148, Japan, and [c]Department of Biological Sciences, Graduate School of Science, Osaka University, Toyonaka, Osaka 560-0043, Japan

Correspondence e-mail: amtanok@mail.ecc.u-tokyo.ac.jp

Received 18 February 2009
Accepted 10 April 2009

PDB References: zinc-bound TTHA1623, 2zwr, r2zwrsf; iron-bound TTHA1623, 2zzi, r2zzisf.

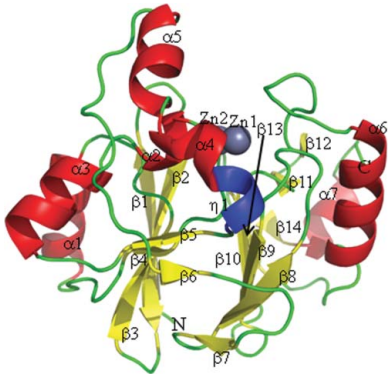

TTHA1623 is a metallo-β-lactamase superfamily protein from the extremely thermophilic bacterium *Thermus thermophilus* HB8. Homologues of TTHA1623 exist in a wide range of bacteria and archaea and one eukaryote, *Giardia lamblia*, but their function remains unknown. To analyze the structural properties of TTHA1623, the crystal structures of its iron-bound and zinc-bound forms have been determined to 2.8 and 2.2 Å resolution, respectively. TTHA1623 possesses an $\alpha\beta\beta\alpha$-fold similar to that of other metallo-β-lactamase superfamily proteins with glyoxalase II-type metal coordination. However, TTHA1623 exhibits a putative substrate-binding pocket with a unique shape.

1. Introduction

TTHA1623 is a metallo-β-lactamase superfamily protein from the extremely thermophilic bacterium *Thermus thermophilus* HB8. The metallo-β-lactamases, which were first identified as class B β-lactamases, possess an $\alpha\beta\beta\alpha$-fold and a di-metal-binding site (Carfi *et al.*, 1995; Concha *et al.*, 1996). Other enzymes with this fold include glyoxalase II, rubredoxin oxygen:oxidoreductase, phosphorylcholine esterase and tRNA maturase. The function of TTHA1623 is unknown, since it possesses neither β-lactamase nor glyoxalase II activity (unpublished data). However, a *BLAST* search has revealed that homologues of TTHA1623 are present in a wide range of bacteria and archaea and one eukaryote (*Giardia lamblia*). Therefore, TTHA1623 and its homologues are likely to play an important role in these organisms. To analyze the structural properties of TTHA1623, we have determined the crystal structures of TTHA1623 in its di-iron-bound and di-zinc-bound forms to 2.8 and 2.2 Å resolution, respectively. TTHA1623 exhibits a uniquely shaped putative substrate-binding pocket with glyoxalase II-type metal coordination (Bebrone, 2007).

2. Materials and methods

2.1. Cloning, expression and purification

The gene encoding TTHA1623 from *T. thermophilus* HB8 (gi:55981592) was amplified by PCR using *T. thermophilus* HB8 genomic DNA as the template. The PCR primers used were 5′-GGA-ATTC**CATATG**AGGGTCTTTCCCGTC-3′ (including an *Nde*I site, shown in bold) and 5′-GA**AGATCT**TATCACGCTTCCCATTCTA-AC-3′ (including a *Bgl*II site, shown in bold). 30 cycles of PCR were performed using KOD-plus (Toyobo, Japan) with a melting phase of 367 K for 30 s, an annealing phase of 326 K for 30 s and a polymerization phase of 341 K for 60 s. The PCR product and the vector plasmid pET-11a(+) (Novagen) were digested by *Nde*I and *Bgl*II and were ligated with Ligation High (Toyobo). The DNA sequence of the TTHA1623-encoding region of the resulting plasmid was verified. The protein without any tags was overexpressed in *Escherichia coli* BL21 (DE3) (Novagen). Harvested cells were resuspended in 20 m*M* Tris–HCl pH 8.0 and 50 m*M* NaCl and then disrupted by sonication.

Table 1
Summary of data-collection and refinement statistics.

Values in parentheses are for the highest resolution shell.

	Zinc-bound crystal				
	1st crystal				
	Zn edge	Zn peak	Zn remote	2nd crystal	Zinc-free iron-bound crystal
Data collection					
Wavelength (Å)	1.2829	1.2822	1.0000	1.0000	1.0000
Resolution range (Å)	50.0–2.40 (2.49–2.40)			50.0–2.20 (2.28–2.20)	50.0–2.80 (2.90–2.80)
No. of observed reflections	125496	136427	139258	125281	69903
No. of unique reflections	36071	37010	37531	26551	12243
Data completeness (%)	96.6 (74.3)	99.9 (99.3)	100.0 (100.0)	99.3 (98.4)	99.8 (100.0)
$R_{\rm merge}$†	0.040 (0.384)	0.041 (0.256)	0.040 (0.239)	0.063 (0.272)	0.096 (0.148)
$\langle I\rangle/\langle\langle\sigma(I)\rangle$	15.5 (1.3)	19.0 (2.7)	20.8 (2.9)	9.1 (2.1)	51.1 (23.3)
Space group	*I*222				$P3_1$
Unit-cell parameters (Å, °)	a = 79.1, b = 114.1, c = 114.7				$a = b$ = 78.6, c = 71.9, $\alpha = \beta$ = 90, γ = 120
Refinement					
Resolution range used for refinement (Å)				50.0–2.20	20.0–2.80
$R_{\rm factor}$‡ (%)				18.8	26.7
$R_{\rm free}$‡ (%)				22.9	29.9
No. of reflections used for refinement				24819	12171
Protein residues modelled				406 of 414	397 of 414
No. of protein atoms modelled				3061	3019
No. of water molecules modelled				158	16
Mean overall B value (Å^2)				16.3	42.0
R.m.s.d. bond angle (°)				1.225	0.895
R.m.s.d. bond length (Å)				0.010	0.005
Ramachandran plot					
Residues in most favoured regions (%)				85.5	82.4
Residues in additionally allowed regions (%)				14.5	17.3
Residues in generously allowed regions (%)				0.0	0.3
Residues in disallowed regions (%)				0.0	0.0

† $R_{\rm merge} = \sum_{hkl}\sum_i |I_i(hkl) - \langle I(hkl)\rangle|/\sum_{hkl}\sum_i I_i(hkl)$. ‡ $R_{\rm factor} = \sum_{hkl} ||F_{\rm o}| - |F_{\rm c}||/\sum_{hkl}|F_{\rm o}|$. $R_{\rm free}$ was calculated using 5% of the data that were excluded from refinement.

The lysate was centrifuged at 40 000*g* at 277 K for 30 min. The supernatant was incubated at 343 K for 10 min and then centrifuged at 40 000*g* at 277 K for 30 min. Ammonium sulfate was added to the supernatant to a final concentration of 1.5 *M*, which was followed by centrifugation at 40 000*g* at 277 K for 30 min. The supernatant solution was loaded onto a Resource ISO (GE Healthcare) column equilibrated with 50 m*M* sodium phosphate buffer pH 7.0 and 1.5 *M* ammonium sulfate. Proteins were eluted with a linear gradient of 1.5–0 *M* ammonium sulfate. The fractions containing TTHA1623 were then loaded onto a hydroxyapatite CHT10 (Bio-Rad) column equilibrated with 10 m*M* sodium phosphate buffer pH 8.0 and eluted with a linear gradient of 10–100 m*M* sodium phosphate pH 8.0. In the final purification step, the fractions containing TTHA1623 were applied onto a HiLoad 16/60 Superdex 75 pg (GE Healthcare) column equilibrated with 20 m*M* Tris–HCl pH 8.0 and 150 m*M* NaCl. The purified TTHA1623 was applied onto a HiPrep 26/10 Desalting (GE Healthcare) column equilibrated with 20 m*M* Tris–HCl pH 8.0 to remove NaCl.

2.2. Crystallization and data collection

The sitting-drop vapour-diffusion method was used for crystallization. 1 µl purified TTHA1623 solution (9.7 mg ml^{-1}) and 1 µl reservoir solution were mixed to prepare a crystallization drop and the drop was equilibrated against 200 µl reservoir solution. Cocrystallization of TTHA1623 with zinc was performed at 293 K with a reservoir solution containing 100 m*M* sodium cacodylate buffer pH 7.3, 30% PEG 200 (Hampton Research) and 200 m*M* zinc acetate. The crystals were picked up in mounting loops and directly frozen in liquid nitrogen without using any cryoprotectant. X-ray diffraction data for the crystals were obtained on beamline BL26B1 at SPring-8 (Harima, Japan). The data for the first crystal were obtained at three wavelengths, the zinc peak (1.2822 Å), edge (1.2829 Å) and remote (1.0000 Å), for use in the zinc multiple-wavelength anomalous dispersion (MAD) method. The data for the second crystal were obtained at 1.0000 Å. Crystallization without zinc was performed at 293 K with a reservoir solution containing 100 m*M* sodium cacodylate pH 6.5 and 1.4 *M* sodium acetate trihydrate. The crystals were picked up in mounting loops and directly frozen in liquid nitrogen using 20% glycerol as the cryoprotectant. The X-ray diffraction data for the zinc-free TTHA1623 crystal were obtained at a wavelength of 1.0000 Å on beamline BL26B1 at SPring-8 (Harima, Japan).

2.3. Structure solution and refinement

The data were processed with the *HKL*-2000 program package (Otwinowski & Minor, 1997) and the *CCP*4 suite (Collaborative Computational Project, Number 4, 1994). The data for the first zinc-bound crystal of TTHA1623 were processed with the 'scale anomalous' flag of *HKL*-2000 to keep Bijvoet pairs separate both in scaling and in the output file; thus, the number of unique reflections for these data sets are double the values for the other data sets (Table 1). Zinc sites were determined with the program *SOLVE* (Terwilliger & Berendzen, 1999) using the MAD data sets of the first crystal and the resulting phases were improved with the program *RESOLVE* (Terwilliger & Berendzen, 1999). Molecular replacement with the program *MOLREP* (Vagin & Teplyakov, 2000) was carried out against the data set obtained from the second crystal using the initial model obtained from the MAD data sets as a search model. The model was refined using *Coot* (Emsley & Cowtan, 2004) and *REFMAC*5 (Murshudov *et al.*, 1997). Using the refined structure of zinc-bound TTHA1623 as the search model, molecular replacement with the program *MOLREP* (Vagin & Teplyakov, 2000) was carried out against the data set obtained from the zinc-free TTHA1623

Table 2
Metal content of TTHA1623.

Each value represents the mean ± standard deviation (n = 3).

Metal ion	Moles of metal per mole of TTHA1623
Fe	1.7 ± 0.0
Mn	0.068 ± 0.001
Zn	0.043 ± 0.002
Cu	0.011 ± 0.000
Mg	<0.010
Al	<0.010
Ca	<0.010
Ni	<0.010

crystal. The model was refined using *Coot* (Emsley & Cowtan, 2004) and *REFMAC*5 (Murshudov *et al.*, 1997). Noncrystallographic symmetry (NCS) restraints were applied throughout the refinement. The stereochemistry of the structure was checked by the program *PROCHECK* (Laskowski *et al.*, 1993).

2.4. Analytical gel filtration

The purified TTHA1623 was loaded onto a Superdex 75 HR 10/30 column (GE Healthcare) equilibrated with 50 m*M* Tris–HCl buffer pH 8.0 and 150 m*M* NaCl and eluted with the same buffer at a flow rate of 0.5 ml min^{-1} at room temperature. The molecular weight of TTHA1623 was estimated by comparing its elution volume with those of the following standard proteins: transferrin (MW 81 000), ovalbumin (MW 43 000), myoglobin (MW 17 600), ribonuclease A (MW 13 700) and aprotinin (MW 6500).

2.5. Metal content analysis

Metal-content analysis of TTHA1623 was carried out with an SPS-1200VR inductively coupled plasma atomic emission spectrometer (ICP-AES; Seiko Instruments) that covered eight types of element (Mg, Al, Ca, Mn, Fe, Ni, Cu and Zn). The purified TTHA1623 was dialyzed against 10 m*M* Tris–HCl pH 8.0 at 277 K overnight to remove loosely bound metal ions and then diluted to 0.5 mg ml^{-1}. The ICP-AES measurements were carried out as described previously (Crowder *et al.*, 1997).

2.6. Structure-similarity search

The structures of TTHA1623 and its homologues were superposed using *DaliLite* (Holm & Park, 2000). The r.m.s.d. value was calculated using the same program.

3. Results and discussion

3.1. Overall structure of zinc-bound TTHA1623

The crystal structure of zinc-bound TTHA1623 was determined at 2.2 Å resolution by a combination of zinc MAD and molecular-replacement methods. The final structure included two protein molecules (residues 1–200 for chain *A* and 1–206 for chain *B* of the 207 residues of the protein), 160 water molecules and 14 zinc ions in the asymmetric unit. No electron density was observed for the remaining residues. Data-collection and refinement statistics are summarized in Table 1. The interface of two TTHA1623 molecules in the asymmetric unit was 290 Å^2, corresponding to only 3% of the total surface area of TTHA1623 and indicating that TTHA1623 was monomeric in the crystal, as shown in solution by gel-filtration chromatography. The TTHA1623 monomer contained 14 β-strands, seven α-helices and one 3_{10}-helix (Fig. 1*a*), and formed a $\beta\beta$-sandwich with helices on each external face, as in other metallo-β-lactamase superfamily proteins (Carfi *et al.*, 1995; Yamamura *et al.*, 2008). The di-metal-binding site is located on one edge of the $\beta\beta$-sandwich, with the two zinc ions located 3.3 Å apart.

3.2. Overall structure and metal content of iron-bound TTHA1623

The crystal structure of TTHA1623 crystallized without the addition of any metal ion was determined at 2.8 Å resolution by the molecular-replacement method. Metal ions were observed in the crystal structure and were determined to be iron using ICP-AES (Table 2). The final structure thus included two TTHA1623 monomers (residues 3–200 for chain *A* and 3–201 for chain *B*), 16 water molecules, four iron ions and two acetate ions in the asymmetric unit. Data-collection and refinement statistics are summarized in Table 1. The interface of two TTHA1623 molecules in the asymmetric unit was 406 Å^2, corresponding to only 5% of the total surface area of TTHA1623. The TTHA1623 monomer contained 14 β-strands, seven α-helices and one 3_{10}-helix (Fig. 1*b*). The di-metal-binding site is located on one edge of the $\beta\beta$-sandwich, with the two iron ions

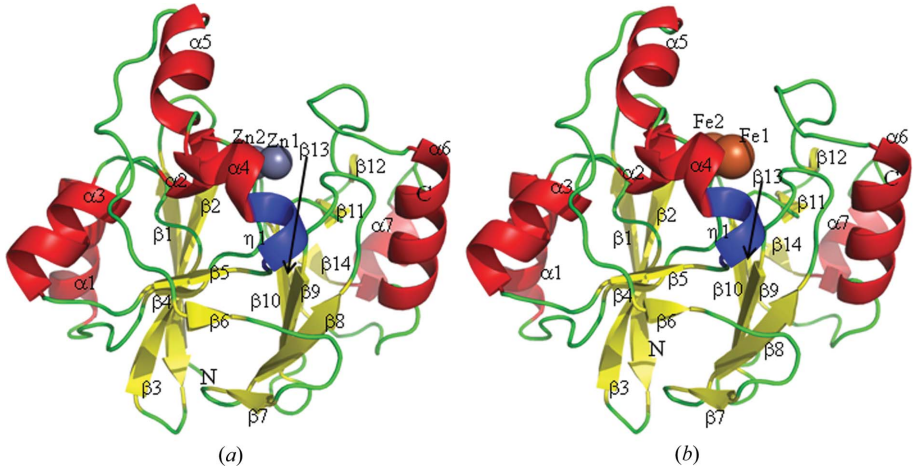

Figure 1
Overall structure of TTHA1623 in di-zinc-bound (*a*) and di-iron-bound (*b*) forms. The N- and C-termini are labelled N and C, respectively. β-strands (β1–14), α-helices (α1–7) and 3_{10}-helix (η1) are shown in yellow, red and blue, respectively. Zinc and iron ions in the putative active site are presented as grey and brown spheres, respectively. This figure was drawn with *PyMOL* (DeLano, 2002).

Table 3
Summarization of *DALI* results.

Z score	PDB code	Source	Protein name	Residues involved in coordination	Metal ions
	2zzi	*T. thermophilus*	TTHA1623	Site 1: His54, His56, His125, Asp144 Site 2: Asp58, His59, Asp144, His184	Site 1: Fe Site 2: Fe
21.6	2q42	*A. thaliana*	Glyoxalase II	Site 1: His54, His56, His112 Site 2: Asp58, His59, Asp131, His169	Site 1: Zn Site 2: Fe
21.6	2gcu	*A. thaliana*	ETHE1-like protein	Site 1: His72, His128, Asp153 Site 2: None	Site 1: Fe
20.2	2qed	*S. typhimurium*	Glyoxalase II	Site 1: His53, His55, His110, Asp127 Site 2: Asp57, His58, Asp127, His165	Site 1: Fe Site 2: Fe
19.7	1qh5	*Homo sapiens*	Glyoxalase II	Site 1: His54, His56, His110, Asp134 Site 2: Asp58, His59, Asp134, His173	Site 1: Zn Site 2: Zn
19.2	2bfz	*B. cereus*	Metallo-β-lactamase	Site 1: His116, His118, His196 Site 2: None	Site 1: Zn

located 3.1 Å apart. The overall structures of di-iron-bound and di-zinc-bound TTHA1623 are almost identical, with an r.m.s.d. of 0.7 Å for the corresponding C^{α} atoms.

3.3. Metal-binding modes of di-zinc-bound and di-iron-bound TTHA1623

In di-zinc-bound TTHA1623, Zn1 was recognized by His54, His56, His125, Asp144 and a water molecule and Zn2 was recognized by Asp58, His59, Asp144, His184 and a water molecule; both formed square-pyramidal coordinations (Fig. 2*a*, left). In di-iron-bound TTHA1623, Fe1 and Fe2 were recognized by the same residues and in the same coordination modes as in di-zinc-bound TTHA1623 (Fig. 2*a*, right). The residues involved in the metal coordination are identical to those in glyoxalase IIs. Interestingly, an acetate was observed 3.0 Å away from Fe2 in the metal-binding site of di-iron-bound TTHA1623. As a result, Fe2 is in a distorted octahedral coordination (Fig. 2*a*, right). It is presumed that the acetate mimics the hydrolyzed product of an amide or an ester, which are the putative substrates of TTHA1623. The acetate was not observed in di-zinc-bound TTHA1623, despite the presence of 200 m*M* zinc acetate in the reservoir solution (Fig. 2*b*).

3.4. Structural similarity search

A structural similarity search was performed with the atomic coordinates of di-iron-bound TTHA1623 using the *DALI* server (Holm & Sander, 1995), as the native TTHA1623 is presumed to bind iron ions. The top five hits were *Arabidopsis thaliana* glyoxalase II (PDB code 2q42; Levin *et al.*, 2007), *A. thaliana* ETHE1-like protein (PDB code 2gcu; McCoy *et al.*, 2006), *Salmonella typhimurium* glyoxalase II (PDB code 2qed; Campos-Bermudez *et al.*, 2007), human glyoxalase II (PDB code 1qh5; Cameron *et al.*, 1999) and *Bacillus cereus* metallo-β-lactamase (PDB code 2bfz; Davies *et al.*,

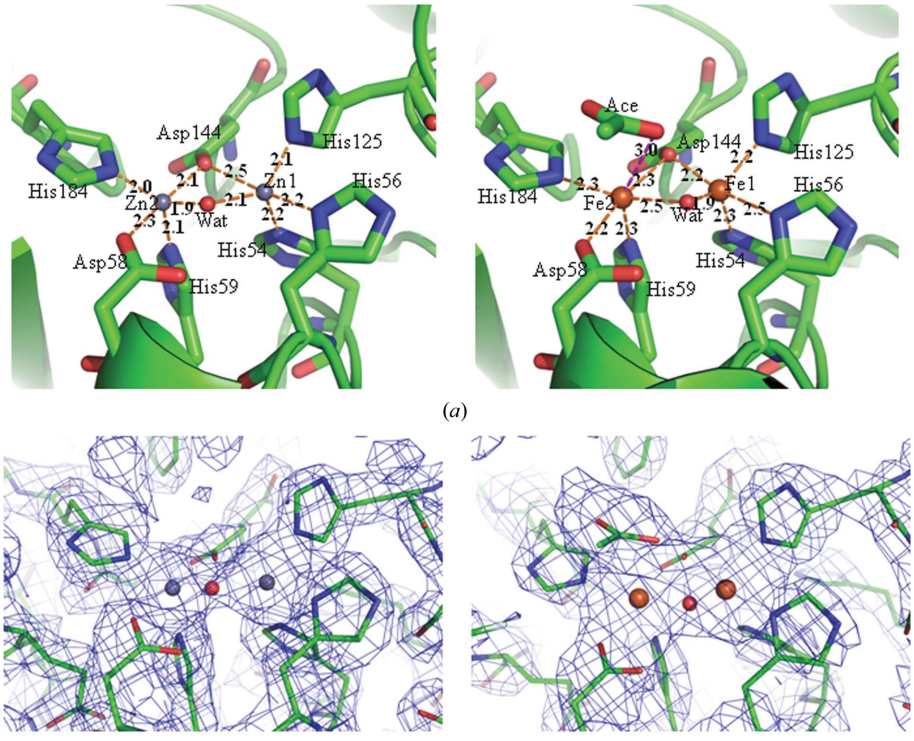

Figure 2
(*a*) The putative active sites of TTHA1623 in di-zinc-bound (left) and di-iron-bound (right) forms. Zinc ions are labelled Zn1 and Zn2 and iron ions are labelled Fe1 and Fe2. The ligand water molecules are shown in red spheres and labelled Wat. The acetate ion is shown in a stick model and labeled as Ace. Dotted lines show the coordination of metal ions by their ligands. The distances between atoms in Å are labeled on the dotted lines. (*b*) σ_A-weighted $2F_o - F_c$ OMIT maps of the putative active sites of TTHA1623 in di-zinc-bound (left) and di-iron-bound (right) forms. The maps are contoured at 1σ. This figure was drawn with *PyMOL* (DeLano, 2002).

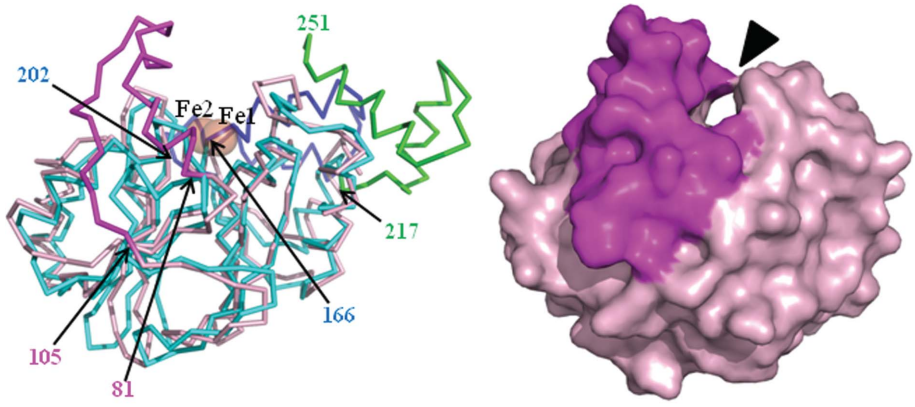

Figure 3
(*a*) Superposed diagram of TTHA1623 (shown in pink) and 2qed (light blue). The region unique to TTHA1623, residues 81–105, is shown in magenta. The regions unique to 2qed, residues 166–202 and 217–251, are shown in blue and green, respectively. The residue numbers of TTHA1623 and 2qed are labelled in the diagram. (*b*) Surface diagram of TTHA1623. The region unique to TTHA1623 (residues 81–105) is shown in magenta and the putative substrate-binding pocket is indicated by an arrowhead. The viewing points of (*a*) and (*b*) are the same. This figure was drawn with *PyMOL* (DeLano, 2002).

2005) (Table 3). The superimposition of TTHA1623 with 2qed, the only di-iron-binding enzyme among the *DALI* hits, was performed using *DaliLite* (Holm & Park, 2000). The $\alpha\beta\beta\alpha$-folds of these metallo-β-lactamase superfamily proteins are similar to each other, with an r.m.s.d. of 1.8 Å between 170 pairs of C^{α} atoms. However, their putative substrate-binding pockets were dissimilar. TTHA1623 lacks residues corresponding to 166–202 and 217–251 of 2qed, which form part of the substrate-binding pocket of 2qed, while 2qed lacks residues corresponding to 81–105 of TTHA1623, which form part of the putative substrate-binding pocket of TTHA1623 (Fig. 3).

4. Conclusion

The present results reveal that (i) TTHA1623 exhibits a uniquely shaped putative substrate-binding pocket with a glyoxalase II-type metal-coordination mode, (ii) the recombinant TTHA1623 protein was in the di-iron-bound form and (iii) the bound iron ions were replaced by zinc ions in the presence of 200 m*M* zinc ions in the environment.

This work was performed under the Structural-Biological Whole Cell Project led by Dr Seiki Kuramitsu at the RIKEN SPring-8 Center. The synchrotron-radiation experiments were performed at BL26B1 at SPring-8 (Harima, Japan). This work was supported by the RIKEN Structural Genomics/Proteomics Initiative (RSGI) and by the National Project on Protein Structural and Functional Analyses and Grants-in-Aid for Scientific Research from the Ministry of Education, Culture, Sports, Science and Technology of Japan.

References

Bebrone, C. (2007). *Biochem. Pharmacol.* **74**, 1686–1701.
Cameron, A. D., Ridderström, M., Olin, B. & Mannervik, B. (1999). *Structure*, **7**, 1067–1078.
Campos-Bermudez, V. A., Leite, N. R., Krog, R., Costa-Filho, A. J., Soncini, F. C., Oliva, G. & Vila, A. J. (2007). *Biochemistry*, **46**, 11069–11079.
Carfi, A., Pares, S., Duée, E., Galleni, M., Duez, C., Frère, J. M. & Dideberg, O. (1995). *EMBO J.* **14**, 4914–4921.
Collaborative Computational Project, Number 4 (1994). *Acta Cryst.* D**50**, 760–763.
Concha, N. O., Rasmussen, B. A., Bush, K. & Herzberg, O. (1996). *Structure*, **4**, 823–836.
Crowder, M. W., Maiti, M. K., Banovic, L. & Makaroff, C. A. (1997). *FEBS Lett.* **418**, 351–354.
Davies, A. M., Rasia, R. M., Vila, A. J., Sutton, B. J. & Fabiane, S. M. (2005). *Biochemistry*, **44**, 4841–4849.
DeLano, W. L. (2002). *The PyMOL Molecular Graphics System.* http://www.pymol.org.
Emsley, P. & Cowtan, K. (2004). *Acta Cryst.* D**60**, 2126–2132.
Holm, L. & Park, J. (2000). *Bioinformatics*, **16**, 566–567.
Holm, L. & Sander, C. (1995). *Trends Biochem. Sci.* **20**, 478–480.
Laskowski, R. A., MacArthur, M. W., Moss, D. S. & Thornton, J. M. (1993). *J. Appl. Cryst.* **26**, 283–291.
Levin, E. J., Kondrashov, D. A., Wesenberg, G. E. & Phillips, G. N. Jr (2007). *Structure*, **15**, 1040–1052.
McCoy, J. G., Bingman, C. A., Bitto, E., Holdorf, M. M., Makaroff, C. A. & Phillips, G. N. (2006). *Acta Cryst.* D**62**, 964–970.
Murshudov, G. N., Vagin, A. A. & Dodson, E. J. (1997). *Acta Cryst.* D**53**, 240–255.
Otwinowski, Z. & Minor, W. (1997). *Methods Enzymol.* **276**, 307–326.
Terwilliger, T. C. & Berendzen, J. (1999). *Acta Cryst.* D**55**, 849–861.
Vagin, A. & Teplyakov, A. (2000). *Acta Cryst.* D**56**, 1622–1624.
Yamamura, A., Ohtsuka, J., Kubota, K., Agari, Y., Ebihara, A., Nakagawa, N., Nagata, K. & Tanokura, M. (2008). *Proteins*, **73**, 1053–1057.